Available online at www.sciencedirect.com
SCIENCE DIRECT®
Journal of Hydrology 276 (2003) 224–239
Journal of Hydrology
www.elsevier.com/locate/jhydrol

Stochastic modeling of transient contaminant transport

Christiana G. Aguirre, Kamyar Haghighi*

Department of Agricultural and Biological Engineering, Purdue University, West Lafayette, IN 1146-47907, USA

Received 26 June 2002; accepted 27 January 2003

Abstract

A stochastic perturbation-based formulation for transient contaminant transport in the vadose zone was developed and implemented. The proposed methodology provides an efficient way to incorporate the small-scale variability of soil properties into large-scale models using effective parameters. A finite element solution of the stochastic differential equation for transient contaminant transport was formulated. The mean concentration value and its variance at each node were evaluated. The advantage of the proposed stochastic finite element approach is that only a few soil parameters are required to describe the variability of its stochastic properties. In addition, the proposed approach is neither site-specific nor contaminant-specific. A one-dimensional transient contaminant transport was simulated and the stochastic results were compared to deterministic and experimental results. The stochastic perturbation-based numerical formulation predicted the velocity of spreading of the contaminant much closer to the experimental measurements, as compared to the deterministic approach.

Keywords: Groundwater; Water quality; Finite element method; Soil; Perturbation; Chemical transport

1. Introduction

Groundwater is one of the most important sources of water, and because of its extensive use, groundwater contamination has become a major environmental concern (Durmusoglu, 2000; Reddy and Lin, 2000). Aquifers supply approximately 19% of the water consumed in the US (Solley et al., 1998). For public supply and domestic use, groundwater supplies approximately 42% of the total (Hudak, 2000).

The quality of groundwater has become a significant concern in the USA and internationally. Agricultural production has come under greater scrutiny for its potential role in the degradation of water resources (Lovejoy et al., 1997). Surface applied agrochemicals are being detected with increasing frequency in groundwaters worldwide (Chu et al., 2000). Detection of these chemicals in drinking water supplies has increased public concern about the safety of the current agricultural practices and techniques used to quickly identify and remediate contaminated groundwater. Prevention of groundwater contamination is absolutely necessary to ensure public safety (Ehteshami et al., 1991).

To evaluate the likelihood of groundwater contamination by agricultural chemicals, various contaminant transport models have been developed to simulate the fate and transport of pollutants in soils and groundwater (Chu et al., 2000; Cunningham et al.,

* Corresponding author.
E-mail address: haghighi@purdue.edu (K. Haghighi).

0022-1694/03/$ - see front matter © 2003 Elsevier Science B.V. All rights reserved.
doi:10.1016/S0022-1694(03)00059-3

1999). Groundwater contamination may often originate in contamination sources that are often located near the soil surface, such as agricultural fields and waste deposits (Jensen and Mantoglou, 1992; Mantoglou, 1992; Russo et al., 2001). Since the contaminant travels first through the vadose zone, it is very important to obtain accurate predictions of the movement of the contaminant in this region. The vadose zone acts as a source of water and solute for the transport processes in the saturated zone (Russo et al., 2001). In this paper, the stochastic perturbation-based approach for contaminant transport through porous media developed by Mantoglou (1984) and Mantoglou and Gelhar (1985) is implemented using a finite element formulation.

In the last 20 years, groundwater research has been focused in developing quantitative models to predict contaminant transport in aquifers. These predictive tools are very important in the investigation and cleanup of contaminated subsurface systems. It is also known that the transport and fate of contaminants are greatly affected by the heterogenity of aquifer properties (e.g. Leblanc et al., 1991).

The prediction of contaminant transport from mathematical models deals with considerable uncertainty due to the presence of heterogeneities in natural soil formations (Zhan and Wheatcraft, 1999; Chang et al., 1999; Wheater et al., 2000; Aguirre et al., 2001; Russo et al., 2001). During the last two decades, stochastic models have been used to quantify the uncertainty in subsurface hydrology (Fiori and Dagan, 1999; Cvetkovic and Dagan, 1994). These models usually deal with stochastic partial differential equations and their analytical solutions, which are restricted to simple geometries, and then, more general numerical approaches are needed for stochastic flow and transport models (Osnes and Langtangen, 1998).

Numerical techniques have been improved drastically but they cannot yield accurate results since the effective large-scale (or field-scale) parameters cannot be accurately determined. This limitation of the standard deterministic modeling approaches, especially in the vadose zone, emphasizes the use of statistical techniques that can incorporate the effects of natural variability of soil parameters (Harter and Yeh, 1998; Aguirre, 2000; Dillah and Protopapas, 2000).

Prediction contaminant movement through an aquifer is crucial when deciding among alternative techniques for remediation (Aguirre, 2000). In order to have reliable predictions, stochastic methodologies are being used more widely in solving flow and contaminant transport in the unsaturated zone (Yeh, 1992; Russo, 1995a,b; Mantoglou and Gelhar, 1989; Zhu and Sykes, 2000; Labolle et al., 2000; Yeh et al., 1985a,b,c; Mantoglou and Gelhar, 1987a,b,c; Harter and Yeh, 1998). Stochastic differential equations can be solved using traditional numerical techniques such as finite differences or finite elements (Nicolai, 1994). The advantages of finite element methods (FEM) over finite differences are many. FEM handle mixed boundary conditions very easily, they can incorporate different material properties and model complex geometries without difficulties (Haghighi et al., 1990; Franca and Haghighi, 1994).

There is an increased need for dealing with large-scale and complicated subsurface problems. In addition, efficiency and accuracy in numerical results are important issues to model developers (Li et al., 2000). The research gap that should be filled is to use efficient and versatile numerical techniques to solve the stochastic differential equations. The use of a stochastic finite element methodology, to deal with contaminant transport in the unsaturated zone, can dramatically improve the efficiency and flexibility of the solution process, and the quality of the results, and can be used as a powerful tool to make an early prediction of the possibility of an environmental disaster.

This paper presents a general finite element methodology for obtaining a large-scale model of transient solute transport in stratified porous media using a stochastic perturbation-based approach. The model assumes the general case of three-dimensional anisotropic heterogeneity with finite local dispersion. It assumes that the scale of variations in hydraulic conductivity exceeds the size of a representative elementary volume (Bear, 1972). A numerical example demonstrates the performance and capability of the proposed numerical model.

2. Stochastic methodology for transient contaminant transport

The stochastic approach used for derivation of the large-scale transport model consists of four basic steps (Bakr et al., 1978; Mantoglou and Gelhar, 1985; 1989;

Gelhar and Axness, 1983; Gelhar et al., 1985; Gelhar, 1993; Aguirre, 2000):

1. The local governing transport equation is averaged over the ensemble of soil property realizations;
2. Cross-correlations between concentration and specific discharge fluctuations are evaluated analytically and then, the expressions for the effective transport parameters are developed;
3. Simplified linearized equations relating concentration fluctuations to specific discharge fluctuations and to soil property fluctuations are derived;
4. The large-scale transport model and the effective macrodispersion parameters are developed.

These steps are briefly summarized below.

2.1. Large-scale model of transient contaminant transport

The governing equation of an ideal non-reactive conservative solute transport in unsaturated flow (assuming constant density and viscosity) is given by:

$$\frac{\partial(\theta c)}{\partial t} = \frac{\partial}{\partial x_i}\left[E_{ij}\frac{\partial c}{\partial x_j} - cq_i\right] \quad i,j = 1,2,3 \tag{1}$$

where c is the concentration of transported solute; θ is the soil moisture content; E_{ij} is the local bulk dispersion coefficient (hydrodynamic dispersion and molecular diffusion are included) and q_i is the local specific discharge.

The unsaturated hydraulic conductivity $K(\psi)$ can be parameterized following the expression proposed by Gardner (1958):

$$\ln K(\psi) = \ln K_s - \alpha\psi \tag{2}$$

where ψ is the capillary tension head output, K_s is the saturated hydraulic conductivity and α is the inclination of $\ln K(\psi)$ vs. ψ.

Assuming that the local soil properties $\ln K_s$ and α the local specific discharge q_i, the concentration c and the soil moisture content θ are realizations of stationary random fields, yields:

$$\ln K_s = F + f \tag{3}$$

$$\alpha = A + a \tag{4}$$

$$q_i = \bar{q}_i + q_i' \quad i = 1,2,3 \tag{5}$$

$$c = \bar{c} + c' \tag{6}$$

$$\theta = \bar{\theta} + \theta' \tag{7}$$

where F, A, $\bar{q}_i$, $\bar{c}$ and $\bar{\theta}$ are the mean values and f a, q_i', c' and θ' are the fluctuations. The mean values are deterministic, smooth spatial functions and the fluctuations are realizations of three-dimensional zero mean second-order stationary random fields.

In order to obtain the large-scale model of transient solute transport in unsaturated soils, Eq. (1) is averaged over the ensemble of realizations of the random fields a and f. Taking the expected value of Eq. (1), yields:

$$\frac{\partial E[\theta c]}{\partial t} = \frac{\partial}{\partial x_i}\left[E_{ij}\frac{\partial E[c]}{\partial x_j}\right] - \frac{\partial E[(cq_i)]}{\partial x_i} = \frac{\partial}{\partial x_i}\left[E_{ij}\frac{\partial \bar{c}}{\partial x_j}\right] - \frac{\partial E[(cq_i)]}{\partial x_i} \tag{8}$$

where $E[\ ]$ is the expected value operator.

Substituting Eqs. (5)–(7) into Eq. (8), the expected value of the last term on the right hand side of Eq. (8) can be rewritten as:

$$E[(cq_i)] = \bar{c}\bar{q}_i + E[c'q_i'] \tag{9}$$

Using Fick's Law yields:

$$E[c'q_i'] = -\hat{E}_{ij}\frac{\partial \bar{c}}{\partial x_j} \tag{10}$$

where $\hat{E}_{ij}$ is the effective bulk macrodispersion coefficient tensor.

Defining a macrodispersivity tensor as:

$$A_{ij} = \frac{\hat{E}_{ij}}{q} \tag{11}$$

where q is the mean specific discharge.

Substituting Eq. (11) into Eq. (10):

$$E[c'q_i'] = -A_{ij}q\frac{\partial \bar{c}}{\partial x_j} \tag{12}$$

Substituting Eqs. (9), (11) and (12) into Eq. (8) and assuming that the fluctuations θ' and c' are small (neglecting the second order terms), yields:

$$\frac{\partial \bar{\theta}\bar{c}}{\partial t} = \frac{\partial}{\partial x_i}\left[(E_{ij} + A_{ij}q)\frac{\partial \bar{c}}{\partial x_j}\right] - \frac{\partial(\bar{c}\bar{q}_i)}{\partial x_i} \tag{13}$$

Eq. (13) is the large-scale transport equation. Comparing Eq. (13) to the local transport Eq. (1), it is noticed that they have a similar form. The term $E_{ij} + A_{ij}q$ is the total large-scale dispersion coefficient. The term $A_{ij}q$, the bulk macrodispersion coefficient defined in Eq. (12), takes into account the dispersion due to the spatial variability of q_i.

2.2. Linearized fluctuation equation

A linearized perturbation equation for steady state conditions relating the concentration fluctuations c' to q_i' is derived substituting Eqs. (5) and (6) into Eq. (1) and taking the expected value:

$$\frac{\partial}{\partial x_i}[\bar{c}\bar{q}_i + E[q_i'c']] = E_{ij}\frac{\partial^2 \bar{c}}{\partial x_i \partial x_j} \tag{14}$$

Subtracting Eq. (14) from the steady-state part of Eq. (1), yields:

$$\frac{\partial}{\partial x_i}[\bar{q}_i c' + q_i'\bar{c} + q_i'c' - E[q_i'c']] = E_{ij}\frac{\partial^2 c'}{\partial x_i \partial x_j} \tag{15}$$

Assuming that the fluctuations c' and q_i' are small, then the second order terms in Eq. (15) may be neglected. The first order approximation for Eq. (15) is then:

$$\frac{\partial}{\partial x_i}[\bar{q}_i c' + q_i'\bar{c}] = E_{ij}\frac{\partial^2 c'}{\partial x_i \partial x_j} \tag{16}$$

Eq. (16) relates the concentration fluctuations c' to the specific discharge fluctuations q_i'.

Fig. 1 shows the coordinate system $x_1'x_2'$ that represents the principal anisotropy axes and the coordinate system x_1x_2 that has the axis x_1 oriented in the direction of the mean specific discharge $\vec{q}$.

The local dispersion tensor for a two-dimensional problem may be written in the form (Bear, 1972):

$$[E_{ij}] = \begin{bmatrix} \alpha_L q & 0 \\ 0 & \alpha_T q \end{bmatrix} \tag{17}$$

where α_L and α_T are the local longitudinal and transversal dispersivities, respectively.

x_1 axis of coordinate system is oriented in the direction of the mean specific discharge $\vec{q}$.

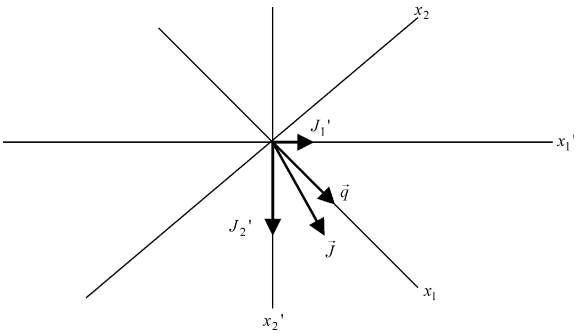

Fig. 1. Coordinate system $x_1'x_2'$ corresponds to the principal anisotropy axes.

Substituting Eq. (17) into Eq. (16) and expanding the left hand side term, yields:

$$q_i'\frac{\partial \bar{c}}{\partial x_i} + q\frac{\partial c'}{\partial x_i} = \alpha_L q\frac{\partial^2 c'}{\partial x_1^2} + \alpha_T q\frac{\partial^2 c'}{\partial x_2^2} \tag{18}$$

Eq. (18) is a linearized differential equation. The mean specific discharge q is given by:

$$q = \sqrt{\hat{K}_{11}J_1' + \hat{K}_{22}J_2'} \tag{19}$$

where $\hat{K}_{ii}$ are the effective hydraulic conductivities given by Aguirre (2000) and J_i' is the mean gradient in the x_i' direction.

The direction of q is given by:

$$\phi = \text{arctg}\left(\frac{\hat{K}_{11}J_1'}{\hat{K}_{22}J_2'}\right). \tag{20}$$

2.3. Evaluation of effective macrodispersion coefficients

The methodology for evaluation of macrodispersivities A_{ij} adopted in this paper was developed by Mantoglou (1984). The methodology utilizes the steady-state linearized fluctuation Eq. (18) and spectral representations. A summary of the results for the general case of statistically anisotropic soil with arbitrary orientation of mean flow is presented next. Two assumptions are necessary in order to get analytical expressions for the macrodispersivities: the soil is supposed to be horizontally stratified and lateral head gradients are considered small.

The macrodispersivities A_{ij} are given by:

$$A_{11} = \frac{\sigma_f^2 \lambda_1 \lambda_2}{\pi \gamma^2 b}(T_{22} + 2\xi^2 T_{23} + \xi^4 T_{33}) \quad (21)$$

$$A_{22} = \frac{\sigma_f^2 \lambda_1 \lambda_2}{\pi \gamma^2 b}\frac{J_2^2}{J_1^2}(\xi^4 T_{33}) \quad (22)$$

$$A_{12} = \frac{\sigma_f^2 \lambda_1 \lambda_2}{\pi \gamma^2 b}\frac{J_2^2}{J_1^2}\xi^2(T_{23} + \xi^2 T_{33}) \quad (23)$$

where:

$$\gamma^2 = \frac{q^2}{K_m^2 J_1^2 \beta^2} \quad (24)$$

$$b = \sqrt{\lambda_1^2(\sin\phi)^2 + \lambda_2^2(\cos\phi)^2} \quad (25)$$

$$\xi^2 = \frac{\lambda_1^2}{\lambda_2^2}(\sin\phi)^2 + (\cos\phi)^2 \quad (26)$$

If a and f are uncorrelated, then

$$\beta^2 = 1 + \xi^2 H^2 \quad (27)$$

If a and f are perfectly correlated, then

$$\beta^2 = 1 - \xi H \quad (28)$$

where H is the mean pressure head and ξ^2 is given by

$$\xi^2 = \frac{\sigma_a^2}{\sigma_f^2}. \quad (29)$$

The gradients J_1 and J_2 are evaluated as:

$$J_1 = J_1' \cos\phi + J_2' \sin\phi \quad (30)$$

$$J_2 = -J_1' \sin\phi + J_2' \cos\phi \quad (31)$$

The integrals T_{22}, T_{23} and T_{33} are evaluated numerically using trapezoid rule (Hoffman, 1992) and they are given by the following expressions:

$$T_{22} = 4\int_0^{\pi/2} \frac{1}{8(a^2-c^2)}\left[\pi - \frac{8c^2}{a^2-c^2}\ln\left(\frac{c^2}{a^2}\right)\right] \times(\cos\phi)^4\,d\phi \quad (32)$$

$$T_{23} = 4\int_0^{\pi/2}\int_0^{\infty} \frac{r^5[1-2(\sin\phi)^2(\cos\phi)^2]}{(a^2r^2+c^2)(1+r^2)^2}dr\,d\phi \quad (33)$$

$$T_{33} = 4\int_0^{\pi/2} \frac{1}{8(a^2-c^2)}\left[\pi - \frac{8c^2}{a^2-c^2}\ln\left(\frac{c^2}{a^2}\right)\right](\sin\phi)^4 d\phi \quad (34)$$

where

$$a^2 = (\cos\phi)^2 + \xi^2(\sin\phi)^2 \quad (35)$$

$$c^2 = A^2 L_2^2 b^2 (\cos\phi)^2 \quad (36)$$

where A is defined by Eq. (4) and L_2 is given by:

$$L_2 = J_2 + \frac{\partial H}{\partial x_i} \quad (37)$$

The prediction of an actual concentration distribution consists of the ensemble mean value and a quantification of the deviation around the mean (σ_c). Vomvoris and Gelhar (1990) derived an analytical expression for the concentration variability in the case of a steady concentration field. This expression was used in this study to approximately quantify the concentration variance for unsteady conditions in unsaturated soils (Aguirre, 2000).

3. Finite element formulation for transient solute transport

The large-scale transient transport model for two-dimensional problems is given by:

$$\frac{\partial \bar{\theta}\bar{c}}{\partial t} = -\left(\bar{c}\frac{\partial \bar{q}_1}{\partial x_1} + \bar{q}_1\frac{\partial \bar{c}}{\partial x_1} + \bar{c}\frac{\partial \bar{q}_2}{\partial x_2} + \bar{q}_2\frac{\partial \bar{c}}{\partial x_2}\right) + \frac{\partial}{\partial x_1}\left[(E_{11} + A_{11}\bar{q})\frac{\partial \bar{c}}{\partial x_1} + (E_{12} + A_{12}\bar{q})\frac{\partial \bar{c}}{\partial x_2}\right] + \frac{\partial}{\partial x_2}\left[(E_{21} + A_{21}\bar{q})\frac{\partial \bar{c}}{\partial x_1} + (E_{22} + A_{22}\bar{q})\frac{\partial \bar{c}}{\partial x_2}\right] \quad (38)$$

Substituting the local dispersion tensor Eq. (17) into Eq. (38), yields:

$$\frac{\partial \bar{\theta}\bar{c}}{\partial t} = -\left(\bar{c}\frac{\partial \bar{q}_1}{\partial x_1} + \bar{q}_1\frac{\partial \bar{c}}{\partial x_1} + \bar{c}\frac{\partial \bar{q}_2}{\partial x_2} + \bar{q}_2\frac{\partial \bar{c}}{\partial x_2}\right) + \frac{\partial}{\partial x_1} \times\left[(\alpha_L q + A_{11}\bar{q})\frac{\partial \bar{c}}{\partial x_1}\right] + 2\frac{\partial}{\partial x_1} \times\left[(A_{12}\bar{q})\frac{\partial \bar{c}}{\partial x_2}\right] + \frac{\partial}{\partial x_2}\left[(\alpha_T q + A_{22}\bar{q})\frac{\partial \bar{c}}{\partial x_2}\right] \quad (39)$$

The system of finite element equations is obtained by applying the Galerkin Method to the large-scale transient contaminant transport Eq. (39). Combining

the element matrices and summing over all the elements using the direct stiffness procedure yields:

$$[P]\{\dot{\bar{c}}\}+[S]\{\bar{c}\}=\{0\} \tag{40}$$

where $[P]$ is the global capacitance matrix, $[S]$ is the global stiffness matrix, $\{\bar{c}\}$ is the mean capillary tension head value and $\{\dot{\bar{c}}\}=\mathrm{d}\{\bar{c}\}/\mathrm{d}t$.

The global system of equations is evaluated using a finite difference approximation in the time domain (Segerlind, 1984):

$$([P]+\beta\Delta t[S])\{\bar{c}\}_{t+\Delta t} = ([P]-(1-\beta)\Delta t[S])\{\bar{c}\}_t \tag{41}$$

Prescribed values along the boundaries are directly introduced in the final system of Eqs. (41):

$$\bar{c}(x_1,x_2)_\Gamma=\bar{c}_\Gamma \tag{42}$$

The set of finite element equations given by Eq. (42) is solved by Gauus Elimination (Taylor and Hughes, 1981).

4. Solution methodology

The solution methodology used to solve transient contaminant transport problems in this study is summarized next:

(a) At $t=0$, the velocity field, chemical concentration distribution and soil properties (mean values, variances and correlation lengths) are given and boundary conditions are specified.
(b) The associated perturbation Eq. (18) is solved analytically using spectral analysis to obtain the macrodispersivities.
(c) The finite element equations for the large-scale transient contaminant transport (13) is solved numerically by Gauss elimination.
(d) Mean chemical concentration values and variances are obtained at each node.
(e) Time is increased and a new velocity field is computed.
(f) The above steps are repeated until $t=t_\mathrm{f}$.

A finite element code (written in Fortran 90 programming language) was developed for the solution of Eq. (41).

5. Steady-state unsaturated flow transient contaminant transport—Etiwanda Field Station

Considerable progress has been made in the last decade in solute transport research. Many theoretical transport models for unsaturated field soil have been proposed but they remain largely untested because very few large-scale solute transport experiments have been conducted under natural field conditions.

The field-scale transport experiment performed by Butters et al. (1989) is briefly described next. The experiment was designed to expand the database for unsaturated zone solute transport on a scale of interest for agricultural and management scenarios, and also to study the solute dispersion below the soil surface. A two year field study of mobile solute transport in the unsaturated zone was conducted over a 0.64 ha area to a depth of 25 m.

5.1. Experimental site

The experimental site is located at the Etiwanda Field Station approximately 15 miles west of Riverside, California. The extent of the unsaturated zone is in excess of 150 m. The soil on the field site is a nearly level Tujunga loamy sand. The texture in the upper 4.5 m was studied by sampling at 0.3 m in five locations across a 0.64 ha area. The results are listed in Table 1. The dominant characteristics are the gravel layer near 1.2 m and the layer of finer textured soil in the neighborhood of 3 m. Several 25 m long continuous soil cores were also taken and revealed a substratum of variable alluvial layers of sands, coarse sands with gravel, and loams. Soil bulk measurements at 30 cm depth intervals to 1.8 m at different locations had a mean of 1.51 g/cm^3 and a standard deviation of 0.38 g/cm^3. The saturated hydraulic conductivity (K_s) of the soil surface was measured at 56 selected points across the field (Butters et al., 1989). The distribution of measured K_s was normal with a mean of 6.15 cm/h and a CV of 44%. Analysis of the spatial structure of K_s revealed a horizontal correlation length-scale of the stochastic component of about 27 m.

The field site was established in 1979 and consists of 1.44 ha covered by sprinkler irrigation and an inner 0.64 ha containing monitoring devices. The field contains 16 sampling locations separated by 20 m and arranged in a mapped 4×4 square grid (Fig. 2).

Table 1
Results of soil texture analysis with USDA textural classification (Butters et al., 1989)

Depth (cm)	Sand (%)	Silt (%)	Clay (%)	Textural classification
30	81	13	6	Loamy sand
60	78	17	5	Loamy sand
90	86	10	4	Loamy sand
120	87	8	5	Gravelly coarse sand
150	81	13	6	Loamy sand
180	76	14	10	Fine sandy loam
210	73	15	12	Fine sandy loam
240	64	22	12	Fine sandy loam
270	54	28	17	Fine sandy loam
300	51	34	15	Loam
330	51	33	15	Loam
360	53	31	16	Sandy loam
390	71	20	9	Fine sandy loam
420	66	24	10	Fine sandy loam
450	71	19	10	Fine sandy loam

Each sampling location contains six ceramic soil solution vacuum samplers, offset by 0.3–0.6 m and are installed at depths of 0.3, 0.6, 0.9, 1.2, 1.8 and 3.05 m. Six of the locations have an additional sampler at 4.5 m. The sprinkler irrigation system over the 1.44 ha plot and border area delivers a flux of 0.05 cm/h. Irrigation collection cups were placed at each of the sampling sites. A cover crop of sorghum and wheat was planted in order to protect the soil from wind erosion and mechanical stress of the excessive sprinkler irrigations.

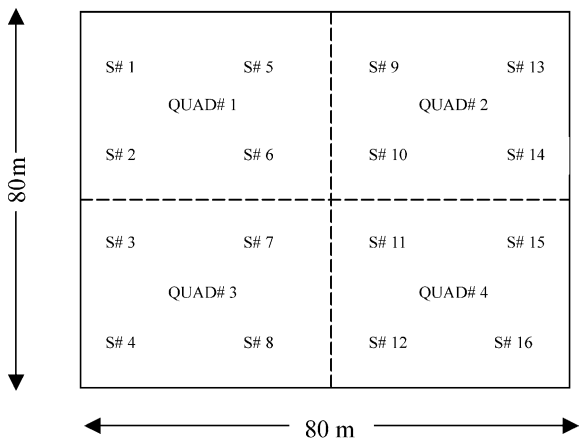

Fig. 2. Sketch of field plot, quadrants and sampling sites (Butters, 1987).

5.2. Experimental method

The field was irrigated regularly for several weeks prior to the tracer application to leach the soil of residual salts from previous experiments and to achieve a reasonably time invariant water content profile to a depth in excess of 3 m. The gravimetric water content θ_g as a function of depth, measured at intervals of 0.15–4.5 m between two irrigation events, is presented in Fig. 3. Temporal variations in the θ_g profile were neglected.

When water could be extracted from all the solution samplers, between 0.3 and 4.5 m, it was assumed that the area-averaged soil water flux was relatively uniform with depth. The inorganic water trace pulse was then injected through the sprinkler system. The 166.5 kg of reagent-grade NaBr were mixed in several 50 gallon drums (1 gallon = 3.785 l) and simultaneously siphoned into the irrigation system in a 30 min period followed by an additional 2.5 h of irrigation. The application mass was 142.9 mmol/m^2 and input concentration of 58.9 mol/m^3. The soil was then leached free of bromide down to 4.5 m over the next nine months by irrigation at 2-day intervals. A field average of 2.32 m of applied irrigation was required over a period of 265 days to leach the bromide tracer past the 450 cm depth at all six solution sampler sites.

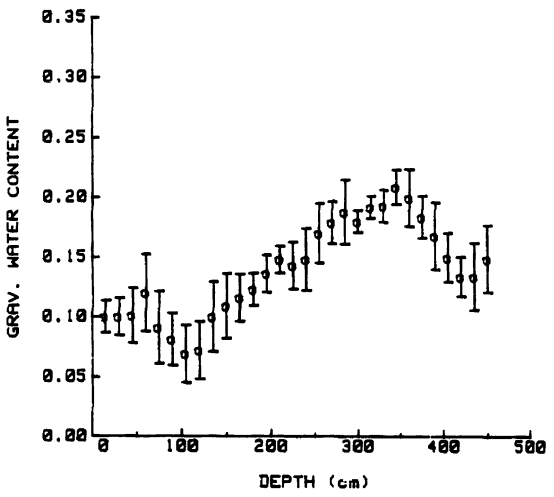

Fig. 3. Steady state gravimetric water content profile estimated from six replicates, along 95% confidence interval (based on t statistic) (Butters et al., 1987).

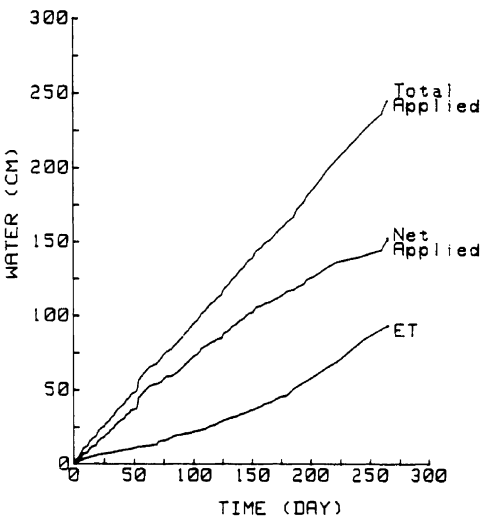

Fig. 4. Water balance for duration of experiment. Water applied is irrigation + precipitation (Butters, 1987).

However, of this total, only the net applied water (NAW) was effective in moving the tracer downward. A plot of cummulative applied water, cumulative evapotranspiration and cumulative NAW vs. time is shown in Fig. 4. The drainage flux is approximated by two values:

$$q_1 = 0.9 \text{ cm/day} \quad \text{for } t < 150 \text{ days} \tag{43}$$

$$q_1 = 0.5 \text{ cm/day} \quad \text{for } t \geq 150 \text{ days} \tag{44}$$

The pressure head distribution through the soil layers was computed using the Van Genuchten expression:

$$h = \frac{1}{\alpha}\left[\left(\frac{\theta - \theta_r}{\phi - \theta_r}\right)^{-1/m} - 1\right]^{1/m} \tag{45}$$

where α is given by the inverse of the bubbling capillary pressure (h_b), θ is the volumetric water content; θ_r is the residual water content; ϕ is the soil porosity; m and n are function of the pore size index (l) and are given by:

$$n = l + 1 \tag{46}$$

$$m = l/n \tag{47}$$

The volumetric water content for each depth is obtained from Fig. 3 by multiplying the gravimetric water content by the dry soil bulk density (1.51 g/cm^3) and dividing by the water density (0.998 g/cm^3). All the others parameters listed above where obtained from Rawls and Brakensiek (1989). The values are presented in Table 2.

Table 2
Hydrologic soil properties

Depth (cm)	ϕ (cm^3/cm^3)	θ_r (cm^3/cm^3)	h_b (cm)	l
30	0.437	0.055	20.58	0.553
60	0.437	0.035	20.58	0.553
90	0.437	0.035	20.58	0.553
120	0.437	0.020	15.98	0.694
150	0.437	0.035	20.58	0.553
180	0.453	0.041	30.20	0.378
210	0.453	0.041	30.20	0.378
240	0.453	0.041	30.20	0.378
270	0.453	0.041	30.20	0.378
300	0.463	0.027	40.12	0.252

The input data used to run the simulations are summarized below in Table 3:

The parameters A, α_a^2 and λ_1 were not measured experimentally. Polmann et al. (1998) performed a literature review to identify whether the spatial data required to estimate the stochastic parameters could be found in papers which describe field soil spatial variability experiments. Many studies involving spatial variability of soil parameters were identified, but most of the papers did not contain information on the parameters required for this model. Parameter A was chosen such that the curve describing the relationship between the unsaturated hydraulic conductivity and pressure head is represented by a smooth

Table 3
Input data

Parameter	Value
K_s (m/day)	1.476
A (m^{-1})	1
σ_a^2 (m^{-2})	0.5266
F	0.3893
σ_f^2	0.1864
λ_1 (cm)	30
α_L (cm)	1
q (cm/day)	Eqs. (43) and (44)
h (cm)	Eq. (45)
Δt (day)	0.005–0.5
Total time of simulation (days)	250
Initial condition c (mol/m^3)	0

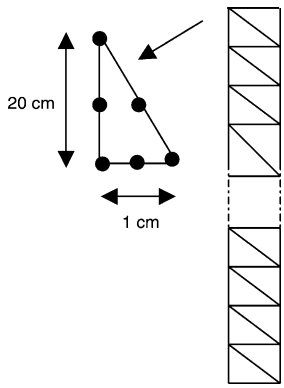

Fig. 5. Finite element mesh: 120 six-noded triangular elements and 305 nodes.

curve. The coefficient of variation used to compute is 44% and is the same as the coefficient of variation measured for the saturated hydraulic conductivity at the soil surface. Vertical correlation length was assumed to be 30 cm to characterize a stratified soil. Vertical correlation length values found in the literature for different types of soils range from 0.08 to 1.8 m (Polmann et al., 1998). All parameters listed in Table 3 are constant values except the drainage flux (Eqs. (43) and (44)) and the initial pressure head distribution (Eq. (45)).

5.3. Results

Local breakthrough curves at different depths were plotted and compared to real breakthrough curves obtained experimentally (Butters, 1987). Numerical results obtained were closer to the experimental results obtained for sampling site number 8 (Fig. 2). This fact may suggest that the values used to characterize the stochastic parameters of the soil are a good approximation of the real values of the soil properties for that specific location. A two-dimensional mesh consisting of 180 six-noded triangular elements and 543 nodes was used (Fig. 5). The vertical domain was extended until 900 cm such that the boundary condition of zero prescribed concentration or $dc/dz = 0$ did not affect the results at $z = 450$ cm.

Fig. 6 shows the local solute breakthroughs at different times as a function of depth. The transport problem was solved using a perturbation and a deterministic approach. The variances of the soil

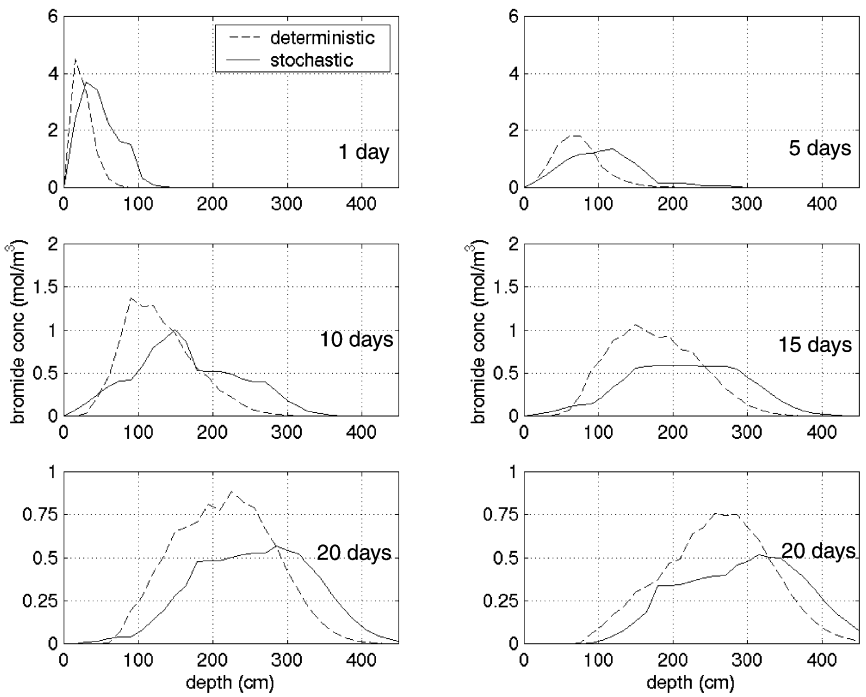

Fig. 6. Bromide concentration vs. depth at different times (deterministic vs. stochastic approaches).

Table 4
Maximum concentration and length of contaminated zone for deterministic and stochastic approaches (% difference = (det − stoch)/stoch × 100)

Time (days)	Maximum concentration (mol/m^3)			Length of contaminated zone (cm)		
	Det	Stoch	% Difference	Det	Stoch	% Difference
1	4.49	3.71	21	90	140	−36
5	1.80	1.34	34	180	270	−33
10	1.37	1.00	37	300	350	−14
15	1.06	0.59	79	350	400	−12
20	0.89	0.56	59	400	450	−11
25	0.76	0.52	46	450	>450	–

properties where set to zero when the deterministic approach was adopted. The dashed lines represent the deterministic results and the solid lines represent the stochastic results. After 1 day, the maximum concentration is 4.49 mol/m^3 for the deterministic approach against 3.71 mol/m^3 for the stochastic approach. The deterministic contaminant front achieves 90 cm and the stochastic contaminant front traveled 140 cm. After 5 days, the peak concentration is around 1.80 mol/m^3 and the contaminant front achieves 180 cm when using the deterministic approach. For the stochastic results, the peak is lower (1.34 mol/m^3) and the contaminated zone extends until 270 cm. After 10, 15 and 20 days, the maximum concentrations for the deterministic results are, respectively, 1.37, 1.06 and 0.89 mol/m^3. For the stochastic approach, the maximum values after 10, 15 and 20 days are, respectively, 1.00, 0.59 and 0.56 mol/m^3. The deterministic contaminant plume extends until 300, 350 and 400 cm after 10, 15 and 20 days, respectively. The stochastic contaminated zone goes further reaching 350, 400 and 450 cm after 10, 15 and 20 days. After 25 days, the maximum concentration is around 0.76 and 0.52 mol/m^3 for the deterministic and stochastic approaches, respectively. The deterministic contaminant zone reaches 450 cm and the stochastic one goes beyond this value. These results and percentage differences are listed in Table 4. The percentage differences show that the deterministic approach predicts a higher maximum concentration and a smaller contaminated zone than the results obtained by using the stochastic approach.

The local solute breakthroughs at different depth as a function of NAW are presented in Fig. 7. At 30 cm depth, the maximum concentration obtained using the stochastic approach is 7.34 mol/m^3 compared to 4.5 mol/m^3 measured experimentally. For 60, 90, 120 and 180 cm depth the maximum concentration values for the stochastic and experimental results are, respectively, 2.30 and 2.50; 2.15 and 1.71; 1.34 and 1.21; 0.59 and 0.49 mol/m^3. At 300 cm depth, the maximum concentrations for the stochastic and experimental results are, respectively, 0.54 and 0.82 mol/m^3. One important parameter to consider when comparing both results is when the contaminant reaches a specific depth and when it is leached from a specific depth. At 30 cm depth, the arrival point is 0 cm of NAW and the contaminant is not present any more after 12 cm of NAW. These values agree for both stochastic and experimental results. At 60 cm depth, the arrival and departure point for both stochastic and experimental results are, respectively, 2.5 and 5 cm NAW; 22.0 and 22.5 cm NAW. At 90 cm depth, the contaminant arrives at 5 cm of NAW and is not present anymore after 31 cm for the stochastic results. The experimental results show that the contaminant arrives at 90 cm depth at 8 cm of NAW and is all leached at 31 cm of NAW. At 120 cm depth, the arrival and departure point for both stochastic and experimental results are, respectively, 8 and 11 cm NAW; 38.0 and 50 cm NAW. At 180 cm depth, the arrival points are 19 and 24 cm of NAW and the contaminant is not present anymore after 80 and 98 cm of NAW, for the stochastic and experimental results, respectively.

Finally, at 300 cm depth, the contaminant arrives at 28 cm of NAW and is not present anymore after 100 cm for the stochastic results. The experimental results show that the contaminant arrives at 300 cm depth at 31 cm of NAW and is all leached at 100 cm of NAW. These results and percentage differences are summarized below (Table 5). The contaminant arrival time is earlier for the stochastic results than for the experimental results. This difference decreases with depth. The time that the contaminant is completely leached from a certain depth is basically the same for both stochastic and experimental results at most depths.

Fig. 8 shows the stochastic results represented by a mean value plus or minus one standard deviation at

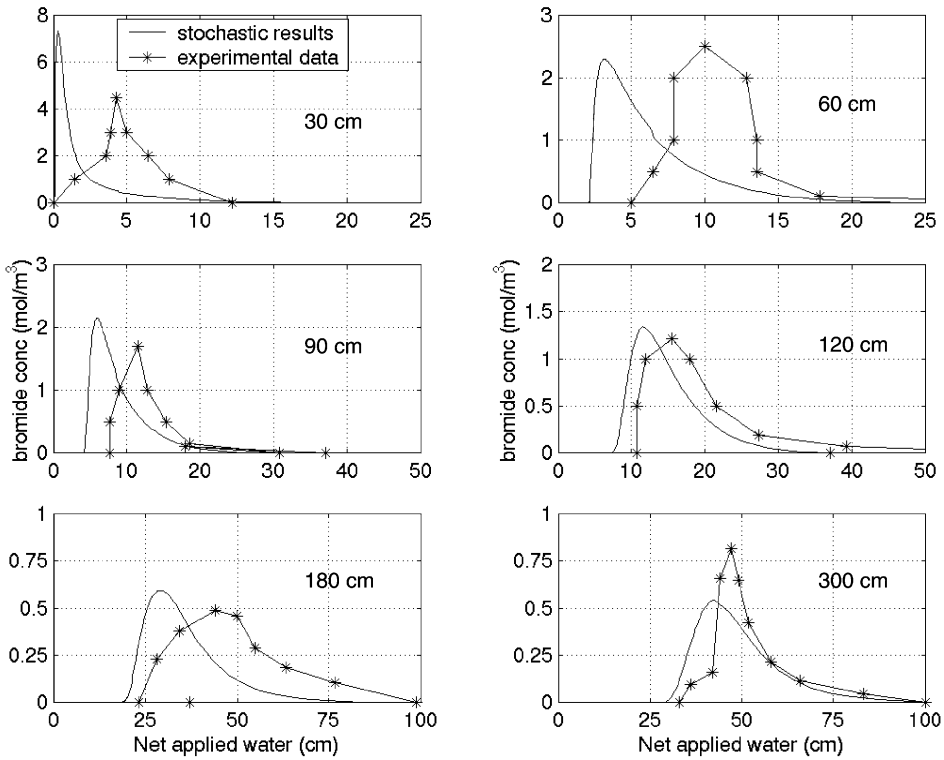

Fig. 7. Bromide concentration vs. NAW at different depths (stochastic vs. experimental results).

different depths. The standard deviation is higher near the maximum concentration values for each one of the BTC. This means that there is a higher uncertainty in these regions compared to the other regions. Since the standard deviation is low, the level of uncertainty is not high enough to make the results unreliable.

A mass balance was performed in order to calculate the solute mass recovered per unit area as a percentage of the total applied mass. Flux concentration is defined as the mass of solute per unit volume of fluid passing through a given cross-section during a short time interval. Mass per unit area M_s is determined by summing the product of the observed solute flux concentration, C_f, and the NAW:

$$M_s = \int_0^{\infty} C_f(z_0, \mathrm{NAW})\mathrm{dNAW} \tag{48}$$

Table 5
Maximum concentration and arrival and end point of contaminant at a specific depth for stochastic approach and experimental results (% difference = (stoch − experim)/experim × 100)

Depth (cm)	Maximum concentration (mol/m^3)			Arrival point (cm NAW)			Ending point (cm NAW)		
	Stoch	Exp	% Difference	Stoch	Exp	% Difference	Stoch	Exp	% Difference
30	7.34	4.50	63	0	0	0	12.0	12.0	0
60	2.29	2.50	−8.4	2.5	5.0	−50	22.0	22.5	−2.2
90	2.15	1.71	25.7	5.0	8.0	−37.5	31.0	31.0	0
120	1.34	1.21	11.0	8.0	11.0	27.3	38.0	50.0	−24.0
180	0.59	0.49	20.4	19.0	24.0	−20.8	80.0	98.0	−18.4
300	0.54	0.82	−34.0	28.0	31.0	−9.7	100.0	100.0	0

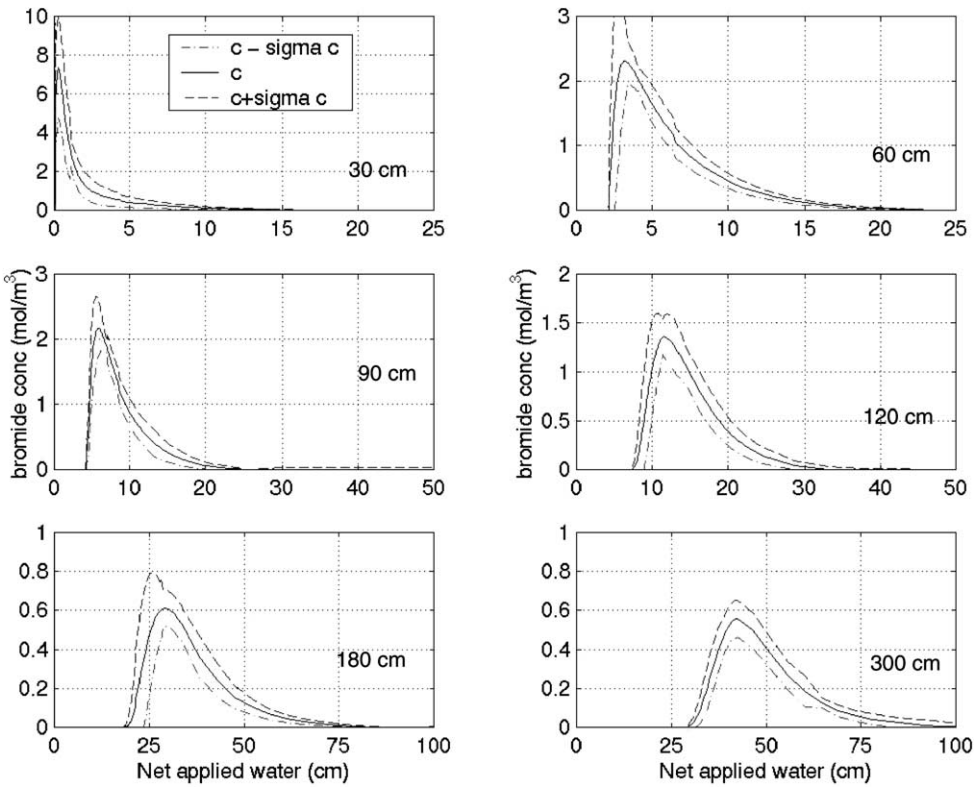

Fig. 8. Mean bromide concentration (±1 standard deviation) vs. NAW at different depths.

The integral in the expression for the mass represents the area under the solute BTC using NAW as the abscissa. The area under the BTC at each depth was estimated numerically using trapezoidal rule (43). Tracer mass applied per unit area was 1.429×10^{-5} mol/cm^2. Results are presented in Table 6. The mass recovery increases with depth and it varies from 76 up to 84%. The expression used for the macrodispersion coefficient was derived for steady state and since this problem is a transient one, the results for earlier times might not be as good as the results for later times. Since the contaminant is moving vertically, it achieves the first layers at early times and as it is shown in Table 6, the mass recovery is the lowest at 30 cm. Other factor that might have contributed to the low

Table 6
Estimated solute mass and mass recovery at each depth

Depth (cm)	Solute mass (M_s), ($\times 10^{-5}$ mol/cm^2) (stochastic)	Mass recovery (%) ($M_s \times 100/1.429 \times 10^{-5}$)	Solute mass (M_{sexp}), ($\times 10^{-5}$ mol/cm^2) (experimental)	Mass recovery (%) ($M_{sexp} \times 100/1.429 \times 10^{-5}$)
30	1.086	75.997	1.670	116.80
60	1.162	81.316	1.606	112.40
90	1.204	84.255	1.035	72.43
120	1.184	82.855	1.467	102.70
180	1.167	81.665	1.644	115.10
300	1.202	84.115	1.193	83.48

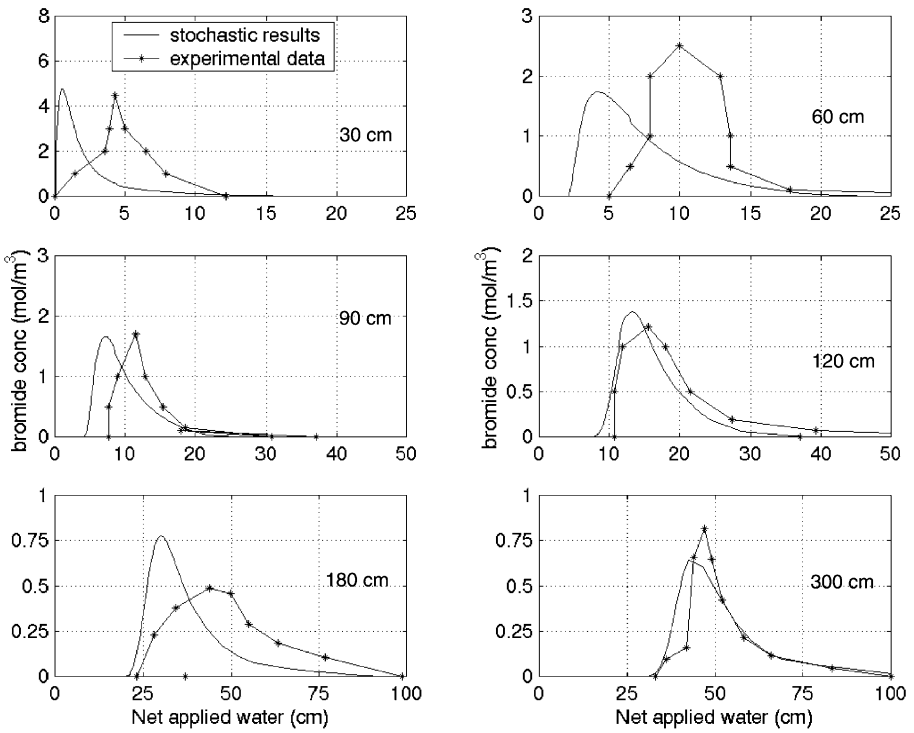

Fig. 9. Bromide concentration vs. NAW at different depths (stochastic vs. experimental results)—optimal BTC.

mass recovery at all depths is that many of the input data values were not measured experimentally in the field. Parameters A, σ_a^2 and λ_1 were not measured experimentally and values available from the literature were assumed. This fact is also a source of error and if the real properties of the soil were used, the recovery mass should be approximately 100% at all depths.

The mass recovery was also evaluated for the experimental data plotted in Fig. 9. The calculated values were more than 100% of recovery for most of depths. Three main reasons can lead to these results. The first one is measurement errors made during the collection of samples to determine the concentration of bromide. The second reason could be the presence of bromide in the soil right before the experiment starts. This means that the soil was not completely leached of bromide prior the beginning of the experiment. The third reason is related to the insufficient number of data points necessary to realistically represent the breakthrough at each depth.

5.4. Sensitivity analysis

A sensitivity analysis was performed in order to improve the numerical results. The variances of stochastic parameters and the vertical correlation length values assumed different values and the

Table 7
Optimal input data

Parameter	Value
K_s (m/day)	1.476
A (m^{-1})	1
σ_a^2 (m^{-2})	0.2
F	0.3893
σ_f^2	0.14
λ_1 (cm)	20
α_{L3} (cm)	1
q (cm/day)	Eqs. (43) and (44)
h (cm)	Eq. (45)
Δt (day)	0.005–0.5
Total time of simulation (days)	250
Initial condition c (mol/m^3)	0

Table 8
Estimated solute mass and mass recovery at each depth

Depth (cm)	Solute mass (M_s) ($\times 10^{-5}$ mol/cm^2) (stochastic)	Mass recovery (%) ($M_s \times 100/1.429 \times 10^{-5}$)	Solute mass (M_{sexp}) (10^{-5} mol/cm^2) (experimental)	Mass recovery (%) ($M_{sexp} \times 100/1.429 \times 10^{-5}$)
30	1.100	76.98	76.00	1.27
60	1.124	78.66	81.32	−3.37
90	1.122	78.52	84.25	−7.30
120	1.210	84.67	82.85	2.14
180	1.347	94.26	81.66	13.36
300	1.355	94.82	84.11	11.29

combination that produced the optimal results (closer to experimental results and mass recovery closer to 100%) were then selected as the optimal input data set (Table 7). The optimal BTCs are presented in Fig. 9. Comparing the optimal BTCs to Fig. 7, the maximum concentration values are closer to the experimental values, except for 60 and 180 cm depths. The arrival and ending points did not change with the new set of input data except for 300 cm depth where these points are now coincident. A mass recovery analysis was preformed under the new set of BTCs and the results are presented in Table 8. The mass recovery basically increases for all depths except for 60 and 90 cm. The mass recovery is around 95% at 180 and 300 cm.

6. Conclusions

A stochastic perturbation-based numerical methodology for transient contaminant transport through unsaturated soils was developed and implemented. The methodology provides an efficient way to incorporate the small-scale variability of the soil properties into large-scale models. Standard deviation of chemical concentration can be evaluated along with the predictions for the mean tension nodal values. The large-scale equation is similar in form to the governing equations of traditional deterministic models. Macrodispersion coefficients depend on the statistical parameters of the intercept ($\ln K_s$) and slope (α) of the local log unsaturated hydraulic conductivity vs. tension function. Site investigations, that are going to implement this methodology, must provide the mean and variance of α (A and σ_a^2), the mean and variance of $\ln K_s$ (F and σ_f^2) and the correlation scales.

A one-dimensional transient contaminant transport was solved using a deterministic and a stochastic approach. This example was used to compare deterministic and stochastic results and verify the stochastic results against real data. The input data necessary to perform the stochastic analysis was not available and values from the literature were assumed. A sensitivity analysis was made in order to get mean BTCs closer to the experimental BTCs and mass recovery closer to 100%. Although the lack of soil property values is a limitation, the stochastic results obtained numerically are in good agreement with experimental results.

The numerical results presented in this study show that the stochastic finite element approach is a very attractive alternative to deterministic approaches in terms of cost, efficiency and accuracy of the results.

Acknowledgements

Christiana Aguirre wishes to thank the Brazilian government agency CNPq for partial support of this study.

References

Aguirre, C.G., 2000. Stochastic finite element modeling of unsaturated flow and solute transport in porous media. PhD dissertation, Purdue University, West Lafayette, IN.

Aguirre, C.G., Haghighi, K., Shirmohammadi, A., Montas, H., Madani, A., 2001. Modeling soil heterogeneity, spatial variability of soil properties and transient flow: stochastic finite element approach. Proceedings of the Second International

Symposium and Exhibition on Preferential Flow, Ala Manoa Hotel, Honolulu, Hawaii. Sponsored by ASAE, St Joseph, MI.

Bakr, A., Gelhar, L.W., Gutjahr, A.L., MacMillan, J.R., 1978. Stochastic analysis of spatial variability in subsurface flows 1. Comparison of one- and three-dimensional flows. Water Resources Research 14 (2).

Bear, J., 1972. Dynamics of Fluids in Porous Media, Dover, New York, 764 pp.

Butters, G.L., 1987. Field scale transport of bromide in unsaturated soil. PhD Dissertation, University of California, Riverside.

Butters, G.L., Jury, W.A., Ernst, F.F., 1989. Field scale transport of bromide in an unsaturated soil 1. Experimental methodology and results. Water Resources Research 25 (7), 1575–1581.

Chang, C.-M., Kemblowski, M.W., Urroz, G.E., 1999. Transient stochastic analysis of biodegradable contaminant transport: first-order decay. Transport in Porous Media 35 (1), 1–14.

Chu, X., Basagaoglu, H., Marino, M.A., Volker, R.E., 2000. Aldicarb transport in subsurface environment: comparison of models. Journal of Environmental Engineering 126 (2), 121–129.

Cunningham, J.A., Goltz, M.N., Roberts, P.V., 1999. Simplified expressions for spatial moments of ground-water contaminant plumes. Journal of Hydrologic Engineering 4 (4), 377–380.

Cvetkovic, V., Dagan, G., 1994. Transport of kinetically sorbing solute by steady random velocity in heterogeneous porous formations. Journal of Fluid Mechanics 265, 189–215.

Dillah, D.D., Protopapas, A.L., 2000. Uncertainty propagation in layered unsaturated soils. Transport in Porous Media 38 (3), 273–290.

Durmusoglu, E., Corapcioglu, M.Y., 2000. Experimental study of horizontal barrier formation by colloidal silica. Journal of Environmental Engineering 126 (9), 833–841.

Ehteshami, M., Peratala, R.C., Eisele, H., Deer, H., Tindall, T., 1991. Assessing pesticide contamination to groundwater: a rapid approach. Ground Water 29 (6), 862–868.

Fiori, A., Dagan, G., 1999. Concentration fluctuations in transport by groundwater: comparison between theory and field experiments. Water Resources Research 35 (1), 105–112.

Franca, A.S., Haghighi, K., 1994. Adaptive finite element analysis of transient thermal problems. Numerical Heat Transfer, Part B 26 (3), 274–294.

Gardner, W.R., 1958. Some steady-state solutions of the unsaturated moisture flow equation with applications to evaporation from a water table. Soil Science 85 (4), 228–232.

Gelhar, L.W., 1993. Stochastic Subsurface Hydrology, Prentice-Hall, Englewood Cliffs, NJ.

Gelhar, L.W., Axness, C.L., 1983. Three-dimensional stochastic analysis of macrodispersion in aquifers. Water Resources Research 19, 161–180.

Gelhar, L.W., Mantoglou, A., Welty, C., Rehfeldt, K.R., 1985. A review of field-scale physical solute transport processes in saturated and unsaturated porous media. Electric Power Research Institute, Research Project 2485-5.

Haghighi, K., Irudayaraj, J., Stroshine, R.L., Sokhansanj, S., 1990. Grain kernel drying simulation using the finite element method. Transactions of the ASAE 33 (6), 1957–1965.

Harter, T., Yeh, T.C.J., 1998. Flow in unsaturated random porous media, nonlinear numerical analysis and comparison to analytical stochastic models. Advances in Water Resources 22 (3), 185–195.

Hoffman, J.D., 1992. Numerical Methods for Engineers and Scientists, McGraw-Hill, New York.

Hudak, P.F., 2000. Regional trends in nitrate content of Texas groundwater. Journal of Hydrology 228, 37–47.

Jensen, K.H., Mantoglou, A., 1992. Application of stochastic unsaturated flow theory, numerical simulations and comparisons to field observations. Water Resources Research 28 (1), 269–284.

Labolle, E.M., Quastel, J., Fogg, E., Gravner, J., 2000. Diffusion processes in composite porous media and their numerical integration by random walks: generalized stochastic differential equations with discontinuous coefficients. Water Resources Research 36 (3), 552–651.

Leblanc, D.R., Garabedian, S., Hess, K., Gelhar, L.W., Quadri, R., Stollenwerk, K.G., Wood, W.W., 1991. Large-scale natural gradient tracer test in sand and gravel, Cape Cod, Massachusetts 1. Experimental design and observe tracer movement. Water Resources Research 27 (5), 895–910.

Li, M.-H., Cheng, H., Yeh, G., 2000. Solving 3D subsurface flow and transport with adaptive multigrid. Journal of Hydrological Engineering 5 (1), 74–81.

Lovejoy, S.B., Lee, J.G., Randhir, T.O., Engel, B.A., 1997. Research needs for water quality management in the 21st century: a spatial decision support system. Journal of Soil and Water Conservation January–February, 18–22.

Mantoglou, A., 1984. Large-scale models of transient unsaturated flow and contaminant transport using stochastic methods. PhD dissertation, MIT.

Mantoglou, A., 1992. A theoretical approach for modeling unsaturated flow in spatially variable soils: effective flow models in finite domains and nonstationarity. Water Resources Research 28 (1), 251–267.

Mantoglou, A., Gelhar, L.W., 1985. Large-scale models of transient unsaturated flow and contaminant transport using stochastic methods. Ralph M. Parsons Laboratory Hydrology and Water Resource Systems, Report number 299.

Mantoglou, A., Gelhar, L.W., 1987a. Stochastic modeling of large-scale transient unsaturated flow systems. Water Resources Research 23 (1), 37–46.

Mantoglou, A., Gelhar, L.W., 1987b. Capillary tension head variance, mean soil moisture content, and effective specific soil moisture capacity of transient unsaturated flow in stratified soils. Water Resources Research 23 (1), 47–56.

Mantoglou, A., Gelhar, L.W., 1987c. Effective hydraulic conductivities of transient unsaturated flow in stratified soils. Water Resources Research 23 (1), 57–67.

Mantoglou, A., Gelhar, L.W., 1989. Three-dimensional unsaturated flow in heterogeneous systems and implications on groundwater contamination: a stochastic approach. Transport in Porous Media 4, 529–548.

Nicolai, B., 1994. Modeling and uncertainty propagation analysis of thermal food processes. Dissertationes de Agricultura, Doctoraatsproefschrift Nr. 264 aan de Faculteit Landbouwkundige en Toegepaste Biologische Wetenschappen van de K.U. Leuven.

Osnes, H., Langtangen, H.P., 1998. An efficient probabilistic finite element method for stochastic groundwater flow. Advances in Water Resources 22 (2), 185–195.

Polmann, D.J., Vomvoris, E.G., McLaughlin, D., Hammick, E.M., Gelhar, L.W., 1998. Application of stochastic methods to the simulation of large-scale unsaturated flow and transport. Massachusetts Institute of Technology.

Rawls, W.J., Brakensiek, D.L., 1989. Estimation of soil water retention and hydraulic properties, Unsaturated Flow in Hydrologic Modeling—Theory and Practice, Kluwer, Dordrecht, pp. 275–300.

Reddy, K.J., Lin, J., 2000. Nitrate removal from groundwater using catalytic reduction. Water Research 34 (3), 995–1001.

Russo, D., 1995a. On the velocity covariance and transport modeling in heterogeneous anisotropic porous formations 2. Unsaturated flow. Water Resources Research 31 (1), 139–145.

Russo, D., 1995b. Stochastic analysis of the velocity covariance and the displacement covariance tensors in partially saturated heterogeneous anisotropic porous formations. Water Resources Research 31 (7), 1647–1658.

Russo, D., Zaidel, J., Laufer, A., 2001. Numerical analysis of flow and transport in a combined heterogeneous vadose zone-groundwater system. Advances in Water Resources 24, 49–62.

Segerlind, L.J., 1984. Applied Finite Element Analysis, Second ed, Wiley, New York.

Solley, W.B., Pierce, R.R., Perlman, H.A., 1998. Estimated use of water in the United States in 1995. United States Geological Survey Circular 1200, 1–71.

Taylor, C., Hughes, T.G., 1981. Finite Element Programming of the Navier–Stokes Equations, Pineridge Press Ltd, Swansea, UK.

Vomvoris, E.G., Gelhar, L.W., 1990. Stochastic analysis of the concentration variability in a three-dimensional heterogeneous aquifer. Water Resources Research 26 (10), 2591–2602.

Wheater, H.S., Tompkins, J.A., Van Leeuwen, M., Butler, A.P., 2000. Uncertainty in groundwater flow and transport modelling—a stochastic analysis of well-protection zones. Hydrological Processes 14 (11), 2019–2029.

Yeh, T.C.J., 1992. Stochastic modeling of groundwater flow and solute transport in aquifers. Hydrological Processes 6, 369–395.

Yeh, T.C.J., Gelhar, L.W., Gutjahr, A.L., 1985a. Stochastic analysis of unsaturated flow in heterogeneous soils 1. Statistically isotropic media. Water Resources Research 21 (4), 447–456.

Yeh, T.C.J., Gelhar, L.W., Gutjahr, A.L., 1985b. Stochastic analysis of unsaturated flow in heterogeneous soils 2. Statistically anisotropic media with variable. Water Resources Research 21 (4), 457–464.

Yeh, T.C.J., Gelhar, L.W., Gutjahr, A.L., 1985c. Stochastic analysis of unsaturated flow in heterogeneous soils 3. Observations and applications. Water Resources Research 21 (4), 465–471.

Zhan, H., Wheatcraft, S., 1999. Uncertainty of one-dimensional ground-water flow in strongly heterogeneous formations. Journal of Hydrologic Engineering 4 (2), 152–159.

Zhu, J., Sykes, J.F., 2000. Stochastic simulations of NAPL mass transport in variably saturated heterogeneous porous media. Transport in Porous Media 39 (3), 289–314.